Direct Band Gap Semi-Conductor Si-Doped Quantum-Dot Solar Cell With AlAs Cap Layers

P.Vishnu Pavan[1], U. Naresh[2], Praveen Kumar Ankathi[3]

[1]*Assistant Professor of ECE, St.Mary's Engineering College, Hyderabad.*

[2] *Assistant Professor of ECE, St.Mary's Engineering College, Hyderabad.*

[3]*Assistant Professor of ECE, St.Mary's Engineering College, Hyderabad.*

(E-mail: p.vishnupavan@gmail.com[1], naresh920u@gmail.com[2], praveen.kumar1412@gmail.com[3])

Abstract— One of the requirements for strong subbandgap pho-ton absorption in the quantum-dot intermediate-band solar cell (QD-IBSC) is the partial filling of the intermediate band. Studies have shown that the partial filling of the intermediate band can be achieved by introducing Si doping to the QDs. However, the existence of too many Si dopants leads to the formation of point defects and, hence, a reduction of photocurrent. In this study, the effect of Si doping on InAs/GaAs QD solar cells with AlAs cap layers is studied. The AlAs cap layers prevent the formation of the wetting layer during QD growth and reduce the Si doping density needed to achieve QD state filling. Furthermore, the passivation of defect states in the QD with moderate Si doping is demonstrated, which leads to an enhancement of the carrier lifetime in the QDs and, hence, the open-circuit voltage.

Keywords— Intermediate-band solar cells (IBSCs), molecular beam epitaxy (MBE), quantum-dot (QD) solar cells.

I. INTRODUCTION

SINCE the concept of the intermediate-band solar cell(IBSC) was proposed in 1997, significant efforts have been made to realize IBSCs with efficiencies that exceed the Shockley–Queisser limit of 31% . The IBSC utilizes a collection of intermediate levels within the band gap, called the intermediate band (IB), to absorb subband gap energy photons. Its potential to exceed the Shockley–Queisser limit and reach the theoretical limit of 63.2% arises from the additional pho-to current generated by the subbandgap photon absorption. One of the candidates for the high-efficiency IBSC is the quantum-dot intermediate-band solar cell (QD-IBSC), which utilizes the discrete nature of the carrier density of states and the band gap tunability of quantum dots (QDs). In a QD-IBSC, the IB is formed by the confined electron states in the QD array.

First, thermal decoupling between the IB and the conduction band (CB) of wetting layer (WL) needs to be achieved. Thermal coupling between the IB and CB enables the carriers to be thermally excited or relaxed between the IB and the CB .This thermal process suppresses the second-photon absorption and lowers the effective band gap energy of the solar cell leading to a reduced open-circuit voltage (V_{oc})

Second, the accumulated strain from the QDs leads to the formation of threading dislocations The strain-induced dislocations across the QD region result in a short minority carrier lifetime and hinders the stacking of QD layers that are needed to maximize the QD photon absorption Studies have shown that strain-induced dislocations can be minimized using a high-growth temperature GaAs spacer layer that separates each QD layer

Furthermore, the performance of IBSCs relies on an IB that is partially filled with electrons .For strong subbandgap photon absorption, the IB needs to have empty states to receive the electrons pumped from the VB and states filled with electrons to pump electrons to the CB. We proposed the use of doping as a method to achieve partial filling of the confined states in the IB. That half-filling of the IB can be realized by doping the capping layers of QDs with Si in InAs/ (Al, Ga) As quantum dot solar cells (QDSCs).

In this paper, the saturation of strain-induced dislocations and QD state filling are demonstrated by direct Si doping of InAs/GaAs QDSCs with AlAs CLs. Previously, the deposition of AlAs CLs on InAs QDs could suppress the formation of the WL [8]. Consequently, the effective band gap of the QDSC was increased, which in turn led to the increase in the thermal activation energy and the V_{OC} . In this study, in addition to the enhancement of the V_{OC} by applying AlAs CLs, a further increase in the V_{OC} by ~44 mV is observed by passivating the defect states with moderate Si doping (6 e/dot). In addition, QD state filling, which is essential for strong two-photon absorption, is observed with significantly lower Si doping densities when compared with that of our previous study.

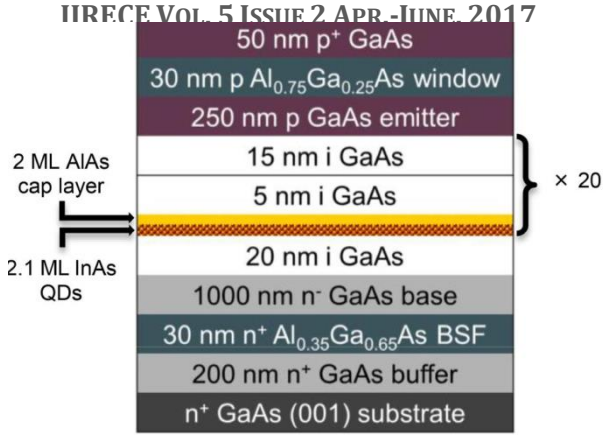

Fig 1. Structure of the Si-doped (0, 6, 12, 18 e/dot) InAs/GaAs QDSCs with AlAs CLs.

II. EXPERIMENTAL DETAILS

The InAs/GaAs QDSC samples with AlAs CLs were grown by a solid-source molecular beam epitaxy (MBE) on n^+ GaAs (1 0 0) substrates. As shown in Fig. 1, all SCs were grown with the same p-i-n structure that consists of a 200-nm GaAs buffer layer with Si doping density of 1×10^{18} cm^{-3}, 30-nm $Al_{0.3\ 5}$ $Ga_{0.6\ 5}$ As back surface field with Si doping density of $1x10^{18}$ cm^{-3}, 1000-nm GaAs base with Si doping density of $1x10^{17}$ cm^{-3}, 250-nm GaAs emitter with Be doping density of 2×10^{18} cm^{-3}, 100-nm GaAs emitter with Be doping density of 5×10^{18} cm^{-3}, 30-nm $Al_{0.\ 7\ 5}$ $Ga_{0.2\ 5}$ As window layer with Be doping density of 2×10^{18} cm^{-3}, and 50-nm GaAs contact layer with Be doping density of 1×10^{19} cm^{-3}. The intrinsic region of the SCs consists of 20 stacks of 2.1 monolayer (ML) InAs QDs with two ML AlAs CLs separated by a 20-nm GaAs spacer. The QDs were grown by the Stranski–Krastanov mode at substrate temperature of ~500 °C. High-growth temperature GaAs spacer layers were applied during the growth of QDs to suppress the formation of dislocations .The QDSCs underwent direct Si doping with four different doping densities of 0, 6, 12, and 18 e/dot.

Prior to device fabrication, the samples were ultrasonicated first in acetone and then in isopropanol for 10 min each. For the surface oxide removal, the samples were immersed in dilute ammonia solution (1:19) for 30 s. A Au-Zn alloy (95% Au, 5% Zn) was thermally evaporated to form a (~200-nm-thick) grid-pattern p-type electrode using a metal shadow mask. For the n-type electrode, 10-nm Ni, 100-nm Au-Ge (88% Au, 12% Ge), 30-nm Ni, and 200-nm Au were thermally evaporated onto the entire back surface and thermally annealed at 400 °C for 60 s in forming gas. No antireflective coating or surface passivation was applied to these SCs.

A Veeco Nanoscope V atomic force microscope (AFM) was used to characterize the morphology of an uncapped QD layer. Temperature-dependent and power-dependent photoluminescence (PL) measurements were performed using 532-nm excitation from a diode-pumped solid-state laser. The sample temperature between 10 and 300 K was controlled using a He-cooled cryostat during the PL measurements. The transient PL measurements were performed with 2-ps pulses at excitation of 750 nm from a mode-locked Ti: sapphire laser that produces an optical pulse train at 76 MHz In addition, a Hamamatsu Synchroscan streak camera C5680 with an infrared enhanced S1 cathode was used for the transient PL signal detection. Current density versus voltage (*J–V*) characteristics were obtained by using an LOT calibrated solar simulator with a xenon lamp under 1-sun air mass (AM) 1.5 G illumination at room temperature. A four point probe station was used to connect devices to a Keithly 2400 source meter that outputs the data to ReRa Tracer 3 software. Photocurrent measurements were performed with a halogen lamp chopped to a frequency of 188 Hz through a Newport monochromator. The monochromatic beam was calibrated with a silicon photodiode, and the data were analyzed with ReRa Photor QE 3.1 software to obtain the external quantum efficiency (EQE) at room temperature.

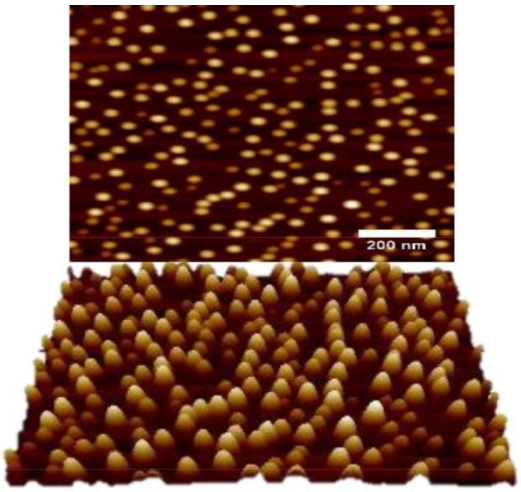

Fig.2. AFM images of InAs QDs grown on GaAs in 2-D (top) and 3-D (bottom).

III. RESULTS AND DISCUSSION

AFM was used to analyze the morphology of InAs QDs on GaAs, as shown in Fig. 2. The average diameter of the QDs was ~30 nm, with an average height of ~5 nm. No large defective clusters were observed, which indicates a high structural quality. The dot density was estimated to be ~2.3×10^{10} cm^{-2}.

The optical properties of the Si-doped InAs/GaAs QDs with AlAs CLs were compared. Fig. 3(a) shows the normalized PL spectra for the QDSCs at 10 K. The PL spectrum of the un-doped QDSC (0 e/dot) shows two peaks at ~830 and ~1050 nm, originating from the GaAs and InAs QD ground state, respectively. The spectra display additional QD emission peaks (950– 1100 nm) for the samples with higher Si doping. This can be explained by the emissions related to excited state transitions observed at shorter wavelengths alongside the ground state emission.

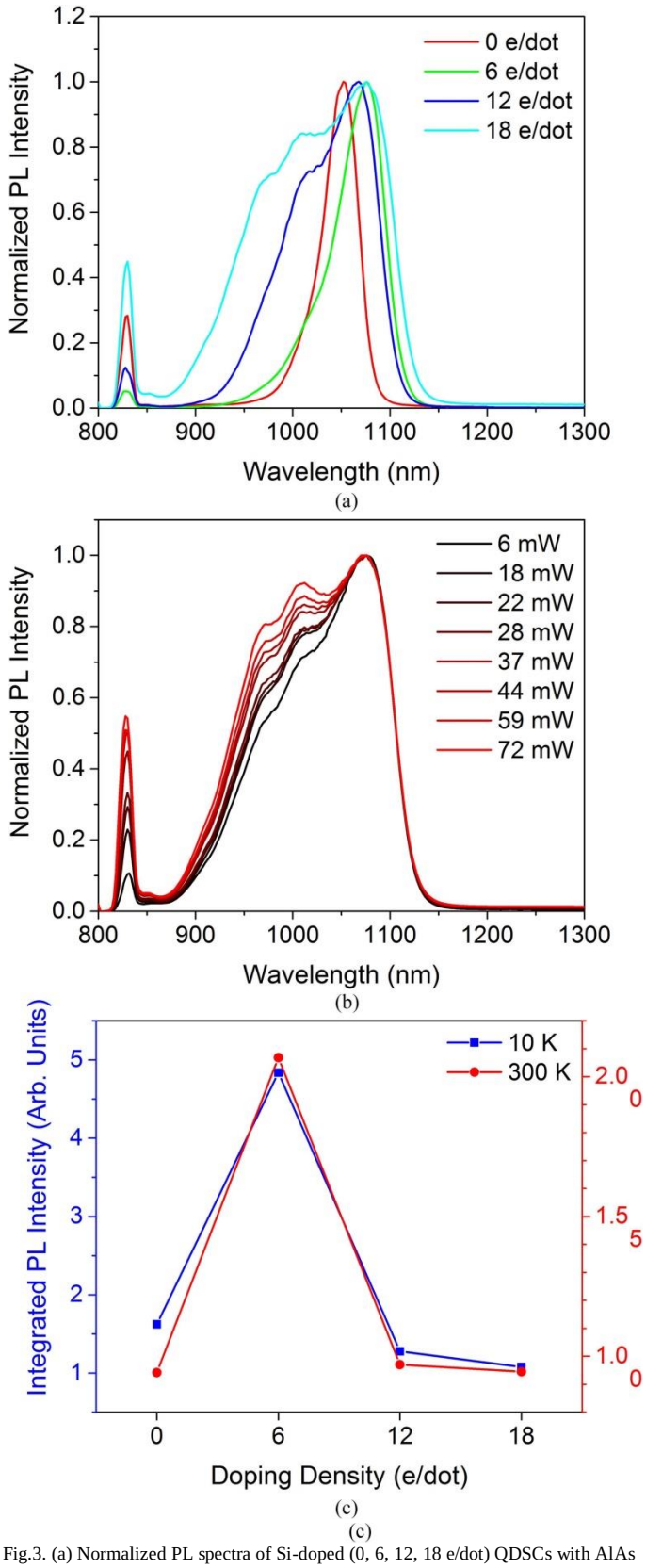

Fig.3. (a) Normalized PL spectra of Si-doped (0, 6, 12, 18 e/dot) QDSCs with AlAs CL measured at 10 K ($P_{e\,x}$ = 37 mW). (b) Normalized power-dependent PL spectra for 18 e/dot QDSC at 10 K. (c) Integrated PL intensity versus Si doping density at 10 K ($I_{e\,x}$ = 386 W/cm^2, $\lambda_{e\,x}$ = 532 nm) and 300 K ($I_{e\,x}$ = 459 W/cm^2 , $\lambda_{e\,x}$ = 635 nm).

Although the higher energy emission peaks can originate from the phonon bottleneck, segregated inhomogeneous broadening, and state filling, it is possible to distinguish them by performing a power-dependent PL study. Fig. 3(b) shows the normalized power-dependent PL spectra for the QDSC with Si doping density of 18 e/dot. It shows that with decreasing laser excitation power, the relative magnitudes of the peaks observed between 950 and 1025 nm decrease, when compared with the peak at ~1080 nm. This indicates that the emission peaks are caused by the state filling effect, where the lowest energy peak is the ground state, and the higher energy peaks are the excited states .The trend that shows excited state emissions become more prominent with higher Si doping density in Fig. 3(a) indicates that the doping results in state filling effect. In our previous study, even though the dopants were directly supplied to the QDs, some dopants remained in the WL and led to a potential barrier forming between the WL and QDs. In contrast, this work prevents the formation of WLs by applying AlAs CLs on QDs during the MBE growth [8]. In this manner, the Si doping is concentrated inside the QDs rather than the WL and contributes to state filling. This explains why the PL peaks from WL emissions that were observed in our previous study with the same Si doping densities are no longer visible, and instead, additional peaks from state filling are observed in Fig. 3(a).

Fig. 3(c) shows the integrated PL intensity as a function of Si doping density at 10 and 300 K. The QDSC with doping density of 6 e/dot exhibits the strongest PL peak intensity. The enhancement of the PL intensity can be attributed to the passivation of the defect states by Si doping and leads to the suppression of nonradiative recombination. However, Fig. 3(c) shows that any further increase in the Si doping level results in a dramatic decrease in the PL intensity. This could be attributed to excess Si atoms that can introduce nonradiative recombination centers .Another possibility is that Si doping introduces additional carriers, which lead to higher Auger recombination rate. In order to provide further evidence of the QD state filling and the passivation of defect states achieved by Si doping, a time-resolved PL study was performed for the QDCSs at 10 K. Fig. 4 shows that the carrier lifetime in the region of 875– 925 nm increases with increasing Si doping density. This can be linked to the state filling effect observed from the steady-state PL measurements in Fig. 3(a). The appearance of the higher energy QD emission peaks with higher Si doping densities in Fig. 3(a) indicates that the additional electrons supplied by the Si dopants are used to fill the QD states. With more QD states filled with electrons, fewer available decay channels exist for the carriers, which in turn results in longer carrier lifetimes. In contrast, the carrier lifetime of the QD ground state (1050–1100 nm) in Fig. 4 shows that increasing the Si doping density leads to an initial increase with moderate doping density (6 e/dot), followed by a significant drop in the carrier lifetime with higher doping densities (12, 18 e/dot). This trend is similar to that observed

in the integrated PL intensity measurements, as shown in Fig. 3(c). Therefore, it can be inferred that the initial increase in the carrier lifetime with doping density of 6 e/dot originates from the passivated defect states. However, once all defect states are filled, further addition of Si atoms leads to the formation of nonradiative recombination centers, and/or increase Auger scattering rate, which decreases the carrier lifetime.

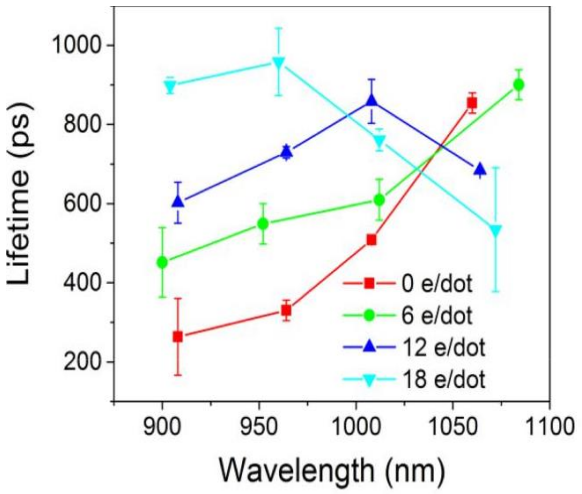

Fig.4. Carrier lifetime versus wavelength obtained from the transient PL spectra of the Si-doped QDSCs with AlAs CLs at 10 K (λ_{ex} = 750 nm).

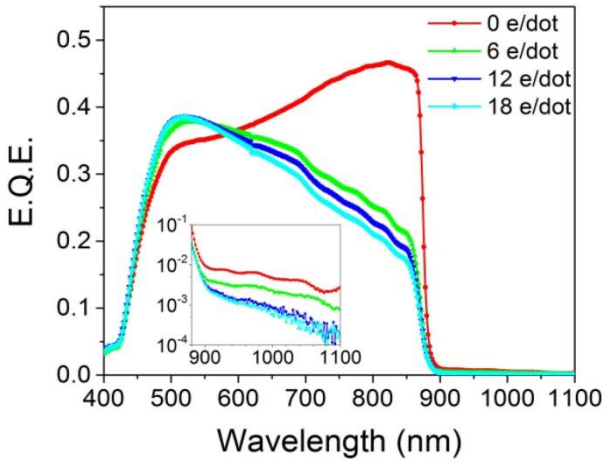

Fig.5. Linear-scale EQE spectra of Si-doped (0, 6, 12, 18 e/dot) QDSCs with AlAs CLs. Inset shows semilog scale of subbandgap EQE

The EQE spectra of the Si-doped QDSCs with AlAs CLs are presented in Fig. 5. For all doped samples, there is a drop in EQE at ~870 nm, which corresponds to the band gap of GaAs. At the higher wavelengths, flat spectral responses without a WL peak (~915 nm) are observed. The subbandgap EQE spectra shown in the inset of Fig. 5 depicts decreasing EQE contribution from the QDs with increasing doping density. This is primarily attributed to the extra electrons introduced by Si doping filling the CB of the QDs, which decreases the probability of the VB to IB transition. As a result, the absorption from the QDs is weakened [13]. Another possibility for the reduced EQE is the suppression of thermal escape of photo excited carriers due to the formation of a potential barrier at QD/WL interface by Si doping, as reported in our previous study [9]. However, with the AlAs CL, it is expected that the formation of such a potential barrier be minimized. It can be also noted from Fig. 5 that the supra-band gap (400–870 nm) absorption of all QDSCs with Si doping is significantly reduced when compared with that of the undoped QDSC. This can be attributed to the decrease in depletion region after Si doping, which reduces the effective absorption area. At the same time, the reduction in the supra-band gap EQE could be linked to the introduction of Si dopants. The Si dopants can substitute the Ga and As sites or exist as interstitial. This leads to the formation of point defects and, hence, a reduction in the EQE response.

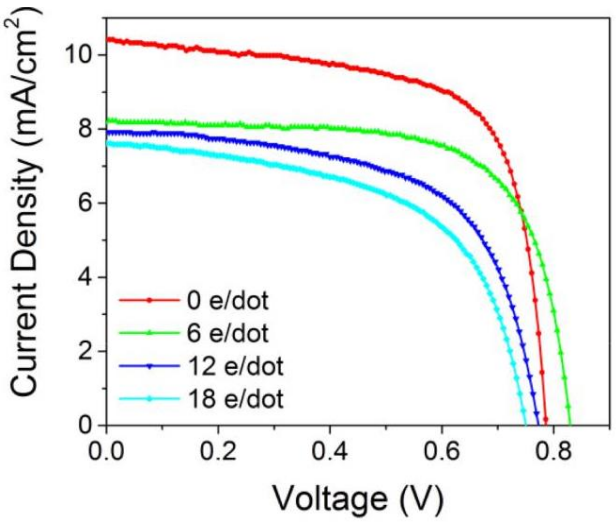

Fig 6. Current density versus voltage behaviour of Si-doped QDSCs with AlAs CLs under 1-sun (AM 1.5G) illumination.

The *J–V* characteristics of the QDSCs in Fig. 6 and Table I show a clear dependence on the Si-doping density. First, all Si-doped samples display a significant drop in the current density when compared with the undoped sample. This can be related to the reduction in the EQE contribution from the supra-band gap region observed in Fig. 5. In other words, the decrease in the depletion region width caused by the introduction of Si dopants results in a reduction in the effective area for absorption and, hence, a decrease in the current density. Second, a further gradual decrease in the current density with increasing doping is observed among the doped QDSCs. This is likely to be due to the point defects formed by Si dopants substituting Ga and As or existing as interstitials. The defect states induced by Si doping increase Shockley–Read–Hall recombination de-crease the minority carrier lifetime and, consequently, lower the current density. Although Si doping has a negative impact in the current density, an enhancement of the V_{OC} is observed with moderate doping density. The V_{OC} increases from 0.783 V for the 0 e/dot QDSC to 0.826 V for the 6 e/dot QDSC. This agrees

well with the trend observed in the PL intensity measurements shown in Fig. 3(c). Both the PL intensity and the V_{OC} reach their maxima at 6 e/dot, which is likely to be due to the moderate Si doping passivating the defect states. However, further increase in the Si doping leads to a gradual decrease in the V_{OC}. This corresponds well with the decreasing PL intensity in Fig. 3(c) that originates from the formation of nonradiative recombination centers due to the excessive concentration of Si atoms.

TABLE I

CURRENT DENSITY, OPEN-CIRCUIT VOLTAGE, FILL FACTOR, AND EFFICIENCY MEASURED FROM SI-DOPED QDSCS WITH ALAS CLS

Device	J_{SC} (mA/cm^2)	V_{OC} (V)	FF (%)	η (%)
0 e/dot	10.41	785.76	68.49	5.60
6 e/dot	8.19	829.34	69.04	4.69
12 e/dot	7.91	772.40	60.69	3.71
18 e/dot	7.61	749.82	56.98	3.25

IV. CONCLUSION

In conclusion, an improvement in the V_{OC} (~44 mV) has been achieved by introducing direct Si doping to QDs with AlAs CLs. The increase in the V_{OC} is attributed to the passivation of the defect states with moderate Si doping (6 e/dot), along with the reduced CB–IB thermal coupling with AlAs CLs. In addition, with the AlAs CLs, the QD state filling effect is ob-served with low Si doping densities. The factors that contributed to the decrease in the supra-band gap EQE and the photocurrent after Si doping, such as the decrease in depletion region and the formation of point defects, should be taken into account when designing future Si-doped QDSCs. Nonetheless, the results presented here hold some promise for overcoming some of the main challenges in implementing QD-IBSCs with the efficiencies close to that of the theoretical model of the IBSC.

REFERENCES

[1] W. Shockley and H. J. Queisser, "Detailed balance limit of efficiency of p-n junction solar cells," J. Appl. Phys., vol. 32, no. 3, pp. 510–519, Mar. 1961.

[2] A. Luque, A. Mart's, and C. Stanley, "Understanding intermediate-band solar cells," Nat. Photon., vol. 6, no. 3, pp. 146–152, Mar. 2012.

[3] S. Sanguinetti et al., "Carrier thermal escape and retrapping in self-assembled quantum dots," Phys. Rev. B, vol. 60, no. 11, pp. 8276–8283, Sep. 1999.

[4] E. Antol´ın et al., "Reducing carrier escape in the InAs/GaAs quantum dot intermediate band solar cell," J. Appl. Phys., vol. 108, no. 6, art. No. 064513, Sep. 2010.

[5] A. Luque and A. Mart's, "The intermediate band solar cell: Progress to-ward the realization of an attractive concept," Adv. Mater., vol. 22, no. 2, pp. 160–174, Nov. 2010.

[6] C. G. Bailey, D. V. Forbes, R. P. Raffaelle, and S. M. Hubbard, "Near 1 V open circuit voltage InAs/GaAs quantum dot solar cells," Appl. Phys. Lett, vol. 98, no. 16, art. no. 163105, Apr. 2011.

[7] A. Mellor, A. Luque, I. Tob´ıas, and A. Mart´ı, "Realistic detailed balance study of the quantum efficiency of quantum dot solar cells," Adv. Funct. Mater. vol. 24, no. 3, pp. 339–345, Jan. 2014.

[8] F. K. Tutu et al., "InAs/GaAs quantum dot solar cell with an AlAs cap layer," Appl. Phys. Lett., vol. 102, no. 16, art. no. 163907, Apr. 2013.

[9] P. Lam et al., "Voltage recovery in charged InAs/GaAs quantum dot solar cells," Nano Energy, vol. 6, pp. 159–166, May 2014.

[10] H. Y. Liu et al., "Improved performance of 1.3μm multilayer InAs quantum-dot lasers using a high-growth-temperature GaAs spacer layer," Appl. Phys. Lett., vol. 85, no. 5, pp. 704–706, Aug. 2004.

[11] F. K. Tutu et al., "Improved performance of multilayer InAs/GaAs quantum-dot solar cells using a high-growth-temperature GaAs spacer layer," J. Appl. Phys., vol. 111, no. 4, art. No. 046101, Feb. 2012.

[12] A. Mart´ı et al., "Emitter degradation in quantum dot intermediate band solar cells," Appl. Phys. Lett., vol. 90, no. 23, art. No. 233510, Jun. 2007.

[13] X. Yang et al., "Improved efficiency of InAs/GaAs quantum dots solar cells by Si-doping," Sol. Energy Mater. Sol. Cells, vol. 113, pp. 144–147, Jun. 2013.

[14] T. Sugaya et al., "Multi-stacked quantum dot solar cells fabricated by intermittent deposition of InGaAs," Sol. Energy Mater. Sol. Cells, vol. 95, no. 1, pp. 163–166, Jan. 2011.

AUTHORS

Mr.P.VISHNU PAVAN is an Assistant Professor of the Electronics and Communication Engineering, St. Mary's Engineering College, Hyderabad .He received his B.Tech degree in Electronics and Communication Engineering from JNT University, Hyderabad, and M.Tech degree in VLSI Design from JNT University, Hyderabad. He is a member of The International Association of Engineers (IAENG).

Mr.U.NARESH is an Assistant Professor of the Electronics and Communication Engineering, St. Mary's Engineering College, Hyderabad .He received his B.Tech degree in Electronics and Communication Engineering from JNT University, Hyderabad, and M.Tech degree in VLSI & Embedded System from JNT University, Hyderabad. He is a member of The International Association of Engineers (IAENG). He had two publications in International Journals.

Mr. PRAVEEN KUMAR ANKATHI is an Assistant Professor of the Electronics and Communication Engineering, St. Mary's Engineering College, Hyderabad .He received his B.Tech degree in Electronics and Communication Engineering from JNT University, Hyderabad, and M.Tech degree in VLSI System Design from JNT University, Hyderabad. He is a member of The International Association of Engineers (IAENG).